Coiling of flexible ropes

By L. Mahadevan[1] and Joseph B. Keller[2]

[1]*Department of Theoretical and Applied Mechanics, University of Illinois at Urbana-Champaign, Urbana, IL 61801, USA*

[2]*Departments of Mathematics and Mechanical Engineering, Stanford University, Stanford, CA 94305, USA*

A thin flexible inextensible rope fed continuously from a fixed height and falling on a horizontal plane usually forms a circular coil. This phenomenon is analysed as a geometrically nonlinear free-boundary problem for a linearly elastic rope. The stiffness and velocity of the rope, the height from which it is fed and gravity are taken into account. The problem is solved by using a numerical continuation scheme. The coil radius is determined as a function of the various parameters. Tables and graphs of the results are presented.

1. Introduction

When an axisymmetric viscous jet falls onto a horizontal surface under the influence of gravity, it coils up in a fairly regular manner (Taylor 1969). A similar phenomenon is observed when a vertical thin flexible rope falls on a rough horizontal surface such as a floor. No satisfactory theoretical analysis has been given for either phenomenon, although there has been some experimental (Griffiths & Turner 1988) and theoretical (Tchavdarov *et al.* 1993) study of the coiling jet. Here we consider the coiling of a flexible rope.

If the rope is fed continuously towards the floor from a fixed height, its motion quickly settles down into a steady state in which the rope is continually laid out in a circular coil of uniform radius. Our goal is to determine the coil radius as a function of the feeding velocity, the stiffness and density of the rope, and the acceleration of gravity.

The behavior of the rope is governed by the dynamic Kirchhoff–Love equations for the motion of an elastic rod capable of large bending and twisting deformations. In terms of these we formulate a free boundary problem for the shape of the rope and the coil radius in § 4. Then we describe a numerical method for the solution of this problem in § 5, and present results for various parameter values. Finally, the asymptotic solution for extreme values of the parameters is examined in § 6.

2. Dimensional analysis

Let us begin with dimensional analysis. There are six parameters: the density ρ of the rope, the Young's modulus E of the material of the rope, the area A and the moment of inertia $I = A^2/2\pi$ of the cross-section (assumed to be circular), the feed velocity v, the height h from which it is fed and the acceleration of gravity g.

Proc. R. Soc. Lond. A (1996) **452**, 1679–1694
Printed in Great Britain

Therefore the number of dimensionless parameters is three, say

$$F = \frac{v^2}{gh}, \quad \gamma = \frac{\rho A g h^3}{EI}, \quad \zeta = \frac{A}{h^2}. \tag{2.1}$$

Here F is the Froude number given by the ratio of the kinetic energy to the gravitational potential energy, γ is the dimensionless gravity given by the ratio of the gravitational and flexural energies, and the dimensionless area ζ is a measure of the rotatory inertia of the rope. The coil radius R can then be written as $R = hf(F, \gamma, \zeta)$.

For thin ropes fed from reasonable heights $\zeta \ll 1$, so that

$$R = hf(F, \gamma, \zeta) \sim hf(F, \gamma, 0). \tag{2.2}$$

We now consider various asymptotic forms of (2.2). If a heavy rope is fed very slowly, the inertial forces are much smaller than the gravitational forces. Then $F \ll 1$, $\gamma = O(1)$, and

$$R \sim hf(0, \gamma, 0) = hg_1(\gamma). \tag{2.3}$$

If R has a finite limit as the feeding height h is increased indefinitely, $g_1(\gamma)$ must be proportional to $\gamma^{-1/3}$. Then (2.3) becomes

$$R \sim Ch\gamma^{-1/3}. \tag{2.4}$$

Here C is a dimensionless constant that can be found from one calculation or one experiment.

On the other hand, if a light rope is fed at moderate velocities, so that the inertial forces are of the same magnitude as gravity, $\gamma \ll 1$ and $F = O(1)$. Then from (2.2) we get

$$R \sim hf(F, 0, 0) = hg_2(F). \tag{2.5}$$

The scaling law (2.4) and the expression (2.5) will serve as checks on the numerical results to be presented in later sections.

For a nylon rope of diameter 0.5 cm, typical parameter values are

$$E \sim 10^{10}\ \mathrm{N\,m^{-2}}, \quad A \sim 10^{-6}\ \mathrm{m^2}, \quad \rho \sim 10^3\ \mathrm{kg\,m^{-3}}. \tag{2.6}$$

If $v \sim 1\ \mathrm{m\,s^{-1}}$ and $h \sim 1\ \mathrm{m}$ then $F \sim 10^{-1}$, $\gamma \sim 1$ and $\zeta \sim 10^{-6}$.

3. Equations of motion

We treat the rope as a naturally straight thin elastic rod of circular cross-section, the centre line of which is parametrized by the arclength s. At any instant of time t, its configuration is given by the position of its centre line and the orientation of its cross-section at every point along it.

At the point s on the centre line of the rod $\boldsymbol{r}(s,t) = (x(s,t), y(s,t), z(s,t))$, we consider an orthogonal triad $\boldsymbol{d}_i(s,t)$, $i = 1, 2, 3$, where $\boldsymbol{d}_1$ and $\boldsymbol{d}_2$ lie along the principal axes of the cross-section of the rod and $\boldsymbol{d}_3 = \boldsymbol{d}_1 \times \boldsymbol{d}_2$. The cross-section of the rod is then characterized by the orientation of $\boldsymbol{d}_i(s,t)$, $i = 1, 2, 3$ relative to a fixed frame $\boldsymbol{e}_i$, $i = 1, 2, 3$. We denote the orthogonal transformation connecting these two frames by $\boldsymbol{L} = \{l_{ij}\}$, so that

$$\boldsymbol{d}_i = \sum_{j=1}^{3} l_{ij}\boldsymbol{e}_j, \quad i = 1, 2, 3. \tag{3.1}$$

The $\{l_{ij}\}$ may be expressed in terms of the Euler parameters, q_0, q_1, q_2, q_3, as described in Appendix A.

For a thin rod, the extensional and shear deformations are small compared to the bending and twisting deformations and may be neglected. Since the cross-section is circular there is no warping. Then the tangent to the centre line of the rope coincides with the normal to the cross-section, so that

$$\boldsymbol{r}_s = \boldsymbol{d}_3, \tag{3.2}$$

where $(\cdot)_s = \mathrm{d}(\cdot)/\mathrm{d}s$.

Differentiating (3.1) yields the spatial rate of change of the director $\boldsymbol{d}_i$, which can be written in terms of the directors as

$$\boldsymbol{d}_{is} = \boldsymbol{k} \times \boldsymbol{d}_i, \quad i = 1, 2, 3. \tag{3.3}$$

The vector of strains $\boldsymbol{k}$ is given by

$$\boldsymbol{k} \equiv \overline{\boldsymbol{L}_s \boldsymbol{L}^T} = \kappa^{(1)} \boldsymbol{d}_1 + \kappa^{(2)} \boldsymbol{d}_2 + \tau \boldsymbol{d}_3. \tag{3.4}$$

Here $\kappa^{(1)}$ and $\kappa^{(2)}$ are the components of the curvature about the $\boldsymbol{d}_1$ and $\boldsymbol{d}_2$ axes, τ is the twist about the centre line, and $\overline{\boldsymbol{L}_s \boldsymbol{L}^T}$ is the axial vector associated with the skew-symmetric matrix $\boldsymbol{L}_s \boldsymbol{L}^T$. The component forms of (3.2) and (3.4) are given in terms of the Euler parameters and their derivatives in Appendix A. This completes the kinematic description of the rod.

The stress resultant vector $\boldsymbol{n}(s,t)$ and the couple resultant vector $\boldsymbol{m}(s,t)$ at any cross-section can be written as

$$\boldsymbol{n}(s,t) = \sum_{i=1}^{3} n^{(i)}(s,t) \boldsymbol{d}_i(s,t), \quad \boldsymbol{m}(s,t) = \sum_{i=1}^{3} m^{(i)}(s,t) \boldsymbol{d}_i(s,t). \tag{3.5}$$

Here, $n^{(1)}$ and $n^{(2)}$ are the shear forces and $m^{(1)}$ and $m^{(2)}$ are the bending moments along the principal axes, while $n^{(3)}$ is the tensile force and $m^{(3)}$ is the twisting moment. The balance of forces and couples at each cross-section yields the equations of motion (Antman 1995)

$$\begin{aligned} \boldsymbol{n}_s + \rho A \boldsymbol{g} &= \rho A \ddot{\boldsymbol{r}}, \\ \boldsymbol{m}_s + \boldsymbol{r}_s \times \boldsymbol{n} &= \rho I \sum_{\iota=1}^{2} (\ddot{\boldsymbol{d}}_\iota \times \boldsymbol{d}_\iota). \end{aligned} \tag{3.6}$$

Here $\boldsymbol{g} = -g\boldsymbol{e}_3$ is the body force per unit length of the rope and $\ddot{\boldsymbol{r}}$ denotes the acceleration relative to an inertial frame.

In analogy with Bernoulli–Euler beam theory, valid for slender rods, we assume that the couple resultant $\boldsymbol{m}(s,t)$ is related to the components of curvature and twist by the linear equation

$$\boldsymbol{m}(s,t) = EI(\kappa^{(1)} \boldsymbol{d}_1 + \kappa^{(2)} \boldsymbol{d}_2) + GJ\tau \boldsymbol{d}_3. \tag{3.7}$$

G is the shear modulus of the material of the rod and J is the polar moment of inertia of the rod cross-section. Equations (3.1)–(3.7) constitute the dynamical Kirchhoff–Love theory for the time-dependent behaviour of a thin elastic rod capable of large deformations.

4. The boundary value problem

We shall consider the motion of a steadily coiling rope. The steady motion consists of a translation of the rope along its tangent at a constant speed v and a rotation about the vertical axis $\boldsymbol{e}_3$ with an angular velocity $\boldsymbol{\Omega} = \Omega \boldsymbol{e}_3$. The inertial accelerations $\ddot{\boldsymbol{r}}$, $\ddot{\boldsymbol{d}}_1$ and $\ddot{\boldsymbol{d}}_2$ induced by this motion are given by

$$\begin{aligned} \ddot{\boldsymbol{r}} &= -[v^2 \boldsymbol{r}_{ss} - 2v\boldsymbol{\Omega} \times \boldsymbol{r}_s + \boldsymbol{\Omega} \times (\boldsymbol{\Omega} \times \boldsymbol{r})] \\ \ddot{\boldsymbol{d}}_\iota &= -[v^2 \boldsymbol{d}_{\iota ss} - 2v\boldsymbol{\Omega} \times \boldsymbol{d}_{\iota s} + \boldsymbol{\Omega} \times (\boldsymbol{\Omega} \times \boldsymbol{d}_\iota)], \quad \iota = 1, 2. \end{aligned} \tag{4.1}$$

Substituting (3.5), (3.7) and (4.1) into (3.6) yields the steady state equations of motion

$$[n^{(1)}\boldsymbol{d}_1 + n^{(2)}\boldsymbol{d}_2 + n^{(3)}\boldsymbol{d}_3]_s + \rho A \boldsymbol{g} = -\rho A[v^2 \boldsymbol{r}_{ss} - 2v\boldsymbol{\Omega} \times \boldsymbol{r}_s + \boldsymbol{\Omega} \times (\boldsymbol{\Omega} \times \boldsymbol{r})], \tag{4.2}$$

$$\begin{aligned} &[EI(\kappa^{(1)}\boldsymbol{d}_1 + \kappa^{(2)}\boldsymbol{d}_2)]_s + [GJ\tau \boldsymbol{d}_3]_s + \boldsymbol{d}_3 \times \sum_{i=1}^{3} n^{(i)}\boldsymbol{d}_i \\ &\qquad = -\rho I \left[\sum_{\iota=1}^{2} (v^2 \boldsymbol{d}_{\iota ss} - 2v\boldsymbol{\Omega} \times \boldsymbol{d}_{\iota s} + \boldsymbol{\Omega} \times (\boldsymbol{\Omega} \times \boldsymbol{d}_\iota)) \times \boldsymbol{d}_\iota \right]. \end{aligned} \tag{4.3}$$

We now define the dimensionless variables

$$\left.\begin{aligned} &\bar{s} = s/l, \quad \bar{x} = x/h, \quad \bar{y} = y/h, \quad \bar{z} = z/h, \\ &\bar{\kappa}^{(1)} = \kappa^{(1)}h, \quad \bar{\kappa}^{(2)} = \kappa^{(2)}h, \quad \bar{\tau} = \tau h, \quad \bar{n}^{(i)} = n^{(i)}h^2/EI, \quad i = 1, 2, 3, \\ &\bar{\Omega} = \Omega h/v, \quad \xi = GJ/EI = 1/(1+\nu), \quad \bar{l} = l/h. \end{aligned}\right\} \tag{4.4}$$

Here h is the drop height, l is the length of the rope between the point of feeding and the point of contact with the horizontal surface, ν is Poisson's ratio and $\Omega = |\boldsymbol{\Omega}|$.

It is convenient to write the equations of motion in component form with respect to the body-convected orthogonal system $\boldsymbol{d}_i$, $i = 1, 2, 3$. In terms of the scaled variables defined in (4.4), and using (3.1) to express the inertial and gravitational terms in the body-convected frame, we can rewrite (4.2)–(4.3), on dropping the bars, as

$$\left.\begin{aligned} l^{-1}n_s^{(1)} - n^{(2)}\tau + n^{(3)}\kappa^{(2)} - \gamma l_{13} &= -F\gamma[\kappa^{(2)} - 2\Omega l_{23} - \Omega^2(xl_{11} + yl_{12})], \\ l^{-1}n_s^{(2)} + n^{(1)}\tau - n^{(3)}\kappa^{(1)} - \gamma l_{23} &= -F\gamma[-\kappa^{(1)} + 2\Omega l_{13} - \Omega^2(xl_{11} + yl_{12})], \\ l^{-1}n_s^{(3)} + n^{(2)}\kappa^{(1)} - n^{(1)}\kappa^{(2)} - \gamma l_{33} &= F\gamma\Omega^2(xl_{31} + yl_{32}), \\ l^{-1}\kappa_s^{(1)} + (\xi - 1)\tau\kappa^{(2)} - n^{(2)} &= \zeta[\ldots], \\ -l^{-1}\kappa_s^{(2)} + (\xi - 1)\tau\kappa^{(1)} - n^{(1)} &= \zeta[\ldots], \\ \xi l^{-1}\tau_s &= 0. \end{aligned}\right\} \tag{4.5}$$

Here the terms multiplied by ζ denote the components of the rotatory inertia in equation (4.3). We assume that the rope is thin, so that $\zeta \ll 1$, and therefore we neglect these terms. Then we use the two penultimate equations in (4.5) to get expressions for $n^{(1)}$ and $n^{(2)}$ in terms of the other variables. Substituting these expressions into the first three equations in (4.5) yields the scaled steady-state equations of motion.

We rewrite these equations, along with the component forms of the kinematic

relations (3.2) and (3.4) (see Appendix A), as

$$\left.\begin{aligned}
l^{-2}\kappa_{ss}^{(1)} &= n^{(3)}\kappa^{(1)} + \gamma l_{23} + F\gamma[\kappa^{(1)} - 2\Omega l_{13} + \Omega^2(xl_{21} + yl_{22})] \\
&\quad +(2-\xi)l^{-1}\tau\kappa_s^{(2)} - (\xi-1)\tau^2\kappa^{(1)}, \\
l^{-2}\kappa_{ss}^{(2)} &= n^{(3)}\kappa^{(2)} - \gamma l_{23} + F\gamma[\kappa^{(2)} - 2\Omega l_{23} - \Omega^2(xl_{11} + yl_{12})] \\
&\quad -(2-\xi)l^{-1}\tau\kappa_s^{(1)} - (\xi-1)\tau^2\kappa^{(2)}, \\
n_s^{(3)} &= -(\kappa^{(1)}\kappa_s^{(1)} + \kappa^{(2)}\kappa_s^{(2)}) + l\gamma[l_{33} + F\Omega^2(xl_{31} + yl_{32})], \quad \tau_s = 0, \\
2q_{1s} &= l(q_0\kappa^{(1)} - q_3\kappa^{(2)} + q_2\tau), \quad 2q_{2s} = l(q_3\kappa^{(1)} + q_0\kappa^{(2)} - q_1\tau), \\
2q_{3s} &= l(-q_2\kappa^{(1)} + q_1\kappa^{(2)} + q_0\tau), \quad 2q_{0s} = l(-q_1\kappa^{(1)} - q_2\kappa^{(2)} - q_3\tau), \\
x_s &= 2l(q_1q_3 + q_0q_2), \quad y_s = 2l(q_2q_3 + q_0q_1), \\
z_s &= l(-q_1^2 - q_2^2 + q_3^2 + q_0^2), \quad s \in [0,1].
\end{aligned}\right\} \tag{4.6}$$

The q_i are the Euler parameters.

To complete the formulation of the problem, we specify the boundary conditions. We assume that the the origin of the coordinate system is directly below the feeding nozzle which is at a height h along the vertical z-axis. In terms of the scaled variables, $\boldsymbol{r}(1) = \boldsymbol{e}_3$, i.e.

$$x(1) = 0, \quad y(1) = 0, \quad z(1) = 1. \tag{4.7}$$

The rope is fed vertically at the feeding point, so that $\boldsymbol{r}_s(1) = \boldsymbol{e}_3$ in the scaled variables. This is equivalent to the condition that the Euler angle $\theta(1) = 0$. From (A 1) it follows that

$$q_1(1) = 0, \quad q_2(1) = 0. \tag{4.8}$$

In the state of steady coiling, the rope assumes a constant shape that revolves around the z-axis with angular velocity Ω, and no twist is induced in the rope as the coils are laid out. We observe that the fourth equation of (4.6) can be integrated to yield $\tau = \text{const}$. Since the rope is free of twist in its natural state, and no twist is introduced at the boundaries, it follows that

$$\tau = 0. \tag{4.9}$$

In a frame rotating with angular velocity Ω about the z-axis, the point of contact of the rope with the plane $z = 0$ is stationary. At this point the rope is tangential to the plane $z = 0$ and to a circle centred at the origin, along which it is laid. This osculating circle to the centre line $\boldsymbol{r}(s)$ of the rope has as its centre $\boldsymbol{c}(s)$, given by (Struik 1988, p. 15)

$$\boldsymbol{c}(s) = \boldsymbol{r}(s) + \kappa^{-1}\boldsymbol{N}(s). \tag{4.10}$$

Here $\kappa(s) = (\kappa^{(1)2} + \kappa^{(2)2})^{1/2}$ is the curvature, and $\boldsymbol{N}(s)$ is the unit normal to the curve, given by

$$\boldsymbol{N}(s) = \kappa^{-1}\boldsymbol{r}_{ss} = \kappa^{-1}\boldsymbol{d}_{3s} = \kappa^{-1}[\kappa^{(2)}\boldsymbol{d}_1 - \kappa^{(1)}\boldsymbol{d}_2]. \tag{4.11}$$

We choose the point of contact $s = 0$ to be on the x-axis, so that the tangent to the rope at $s = 0$ is along the y-axis. Then the Euler angles at $s = 0$ are $\psi(0) = \frac{1}{2}\pi$, $\theta(0) = \frac{1}{2}\pi$ and $\phi(0) = 0$, or equivalently, following (A 1),

$$q_1(0) = -\tfrac{1}{2}, \quad q_2(0) = \tfrac{1}{2}, \quad q_3(0) = \tfrac{1}{2}, \quad q_0(0) = \tfrac{1}{2}. \tag{4.12}$$

Substituting these values into (A 3) and the result into (3.1) yields expressions for $\boldsymbol{d}_i(0)$, $i = 1, 2, 3$ in terms of $\boldsymbol{e}_i(0)$, $i = 1, 2, 3$. Using these expressions in (4.11) and the result in (4.10) gives us three equations for the centre of the osculating circle.

To use these equations we recall that the centre of osculation of the rope at $s = 0$ is the origin $(0, 0, 0)$. This allows us to write (4.10) in dimensionless form as

$$x(0) + \frac{\kappa^{(1)}(0)}{\kappa^2(0)} = 0, \quad y(0) = 0, \quad z(0) - \frac{\kappa^{(2)}(0)}{\kappa^2(0)} = 0. \tag{4.13}$$

By our choice of the point of contact, $y(0) = z(0) = 0$. Substituting this into (4.13), and recalling that $\kappa^2 = \kappa^{(1)2} + \kappa^{(2)2}$, yields the following conditions:

$$y(0) = 0, \quad z(0) = 0, \quad \kappa^{(2)}(0) = 0, \quad \kappa^{(1)}(0)x(0) = -1. \tag{4.14}$$

Assuming that the rope does not slip after contacting the plane, all of it is laid out along the osculating circle. Since the velocity of the contact point is $v\boldsymbol{e}_2$ and the rope steadily rotates about the z-axis with an angular velocity Ω, continuity requires that $\boldsymbol{\Omega} \times \boldsymbol{r}(0) = \Omega \boldsymbol{e}_3 \times x(0)\boldsymbol{e}_1 = v\boldsymbol{e}_2$. Rewriting this in dimensionless form gives

$$\Omega x(0) = 1. \tag{4.15}$$

The system of differential equations (4.6), along with the boundary conditions (4.7)–(4.9), (4.12), (4.14), (4.15), constitutes a thirteenth-order nonlinear two-point boundary value problem. It contains the two given parameters F and γ, and the unknown parameters Ω and l. The unknown variables $\kappa^{(1)}$, $\kappa^{(2)}$, $n^{(3)}$, τ, q_1, q_2, q_3, q_0, x, y and z are functions of s.

5. Numerical solution

To solve the nonlinear boundary value problem posed in § 4 we use a continuation method in which we follow the solution as the parameters F and γ are varied. This requires an initial solution for some particular values of F and γ, which we choose to be $\gamma = F = 0$. For these values, a solution to (4.6) is given by

$$\left.\begin{aligned} x(s) = 1 - \sin\tfrac{1}{2}\pi s, \quad y(s) = 0, \quad z(s) = 1 - \cos\tfrac{1}{2}\pi s, \\ \kappa^{(1)}(s) = 0, \quad \kappa^{(2)}(s) = -1, \quad \tau(s) = 0, \quad n_3(s) = 0, \quad q_0(s) = 0, \\ q_1(s) = -\sin\tfrac{1}{4}\pi(1-s), \quad q_2(s) = 0, \quad q_3(s) = \cos\tfrac{1}{4}\pi(1-s), \quad \Omega = 1, \quad l = \tfrac{1}{2}\pi. \end{aligned}\right\} \tag{5.1}$$

This solution corresponds to a static rope of dimensionless length $\frac{1}{2}\pi$ lying in the x–z-plane, with its ends at $(0, 0, 1)$ and $(1, 0, 0)$. Since $\gamma = 0$, gravity is absent and the rope forms a quarter-circle.

This solution (5.1) does not satisfy all the boundary conditions at $s = 0$. Therefore, we introduce a family of boundary conditions at $s = 0$ with three parameters $\alpha \in [0, 1]$, $\beta \in [0, \pi/2]$ and $\sigma \in [0, 1]$ and replace the boundary conditions (4.12), (4.14), (4.15) by

$$\left.\begin{aligned} \alpha(x(0)\kappa^{(1)} + 1) + (1-\alpha)(x(0)\kappa^{(2)} + 1) = 0, \\ \Omega x(0) = 1, \quad y(0) = 0, \quad z(0) = 0, \\ q_1(0) = 2^{-1/2}\cos\tfrac{1}{2}\beta, \quad q_2(0) = -2^{-1/2}\sin\tfrac{1}{2}\beta, \\ q_3(0) = 2^{-1/2}\cos\tfrac{1}{2}\beta, \quad q_0 = 2^{-1/2}\sin\tfrac{1}{2}\beta, \\ \sigma\kappa^{(2)} + (1-\sigma)\left(\mu - \tfrac{2}{\pi}\right) = 0. \end{aligned}\right\} \tag{5.2}$$

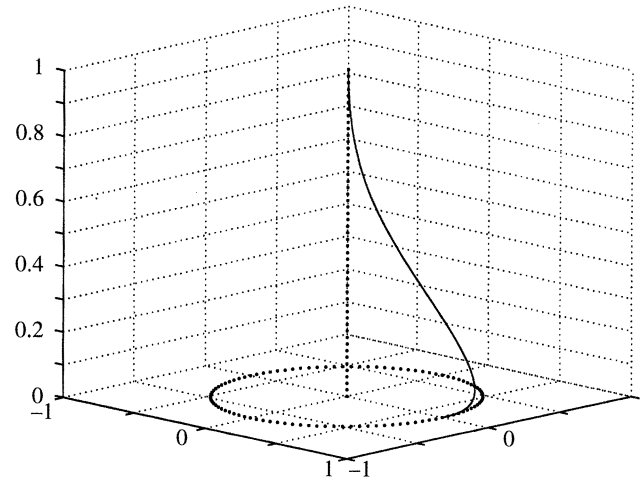

Figure 1. The instantaneous shape of a steadily coiling rope fed very slowly with negligible gravity, so that $F = 0$, $\gamma = 0$. The values of l and R are found to be $l = 1.7921$ and $x(0) \equiv R = 0.6811$.

The parameters α, β and σ characterize the direction of the tangent to the rope at $s = 0$. We observe that when $\alpha = 1$, $\beta = \frac{1}{2}\pi$, $\sigma = 1$, (5.2) is equivalent to (4.12), (4.14), (4.15), while for $\alpha = \beta = \sigma = 0$, we get the boundary conditions satisfied by the quarter-circle solution (5.1). Thus, we can obtain a solution to the boundary value problem posed in § 4 from the quarter-circle solution (5.1) by changing these parameters gradually. This is a continuation or homotopy method.

At each step of the continuation scheme we use AUTO (Doedel 1986), a numerical package for continuation and bifurcation analysis of boundary value problems, to compute the solution. In the absence of bifurcation and turning or fold points, the continuation algorithm simply involves solving a sequence of nonlinear problems. Then each solution gives an initial approximation to the solution at the next step.

To follow the continuation path, we start with the exact solution (5.1) for $\gamma = 0$, $F = 0$ and $\alpha = \beta = \sigma = 0$ and increase β in steps of $\frac{1}{10}\pi$, solving a nonlinear problem at each step. On a uniform mesh with 10 subintervals, the quasi-Newton method takes two iterations per continuation step when the error tolerances on the coordinates x, y and z are 10^{-5}. Once $\beta = \frac{1}{2}\pi$, we keep it fixed at that value and use α as a new continuation parameter, gradually increasing it from its value $\alpha = 0$ till $\alpha = 1$. Finally, we increase σ from its value $\sigma = 0$ till $\sigma = 1$ in a third continuation scheme. In this manner, we obtain the solution to the original boundary value problem for $\gamma = 0$ and $F = 0$. This corresponds physically to the zero-gravity zero-velocity limit of a coiling rope, the centre line of which is shown in figure 1.

To determine the solution for non-zero values of F and γ, we start with the solution just obtained for $F = \gamma = 0$ and use the continuation method again. We first follow the solution as γ is changed in small increments from $\gamma = 0$ to the desired value, say $\gamma = \gamma_1$, keeping $F = 0$ fixed. Then, fixing $\gamma = \gamma_1$, we follow the solution branch by changing F in small increments from $F = 0$ to the desired value, say $F = F_1$. This two-parameter continuation scheme is implemented in AUTO (Doedel 1986), and allows us to determine the dependence of the solution on γ and F. In particular, the variation of the angular velocity $\Omega = 1/R$ and the dimensionless rope length l can be determined.

In tables 1 and 2, we present the dimensionless coil radius $x(0) \equiv R$ and the

Table 1. *The dimensionless coil radius $R = x(0)$ for various values of γ and $F\gamma$*

	$\gamma = 10$	$\gamma = 10^2$	$\gamma = 10^3$	$\gamma = 10^4$
$F\gamma = 1$	0.4386	0.2480	0.1293	0.0659
$F\gamma = 10$	0.4174	0.2301	0.1219	0.0643
$F\gamma = 10^2$	0.6857	0.2510	0.1012	0.0529
$F\gamma = 10^3$	1.1622	0.5058	0.1614	0.0486

Table 2. *The dimensionless rope length l for various values of γ and $F\gamma$*

	$\gamma = 10$	$\gamma = 10^2$	$\gamma = 10^3$	$\gamma = 10^4$
$F\gamma = 1$	1.5117	1.2617	1.1193	1.0163
$F\gamma = 10$	1.5808	1.2742	1.1196	1.0549
$F\gamma = 10^2$	3.2500	1.4605	1.1355	1.0675
$F\gamma = 10^3$	9.5785	3.8037	1.5105	1.0770

dimensionless rope length l for different values of γ and $F\gamma$. Reading table 1 vertically, we observe that for a light rope, i.e. $\gamma = 10$, the radius of the coil initially decreases but then increases as the velocity of feeding, characterized by F, is increased. For moderately heavy ropes, i.e. $\gamma = 10^2$ or 10^3, a similar trend is seen but is delayed until F becomes sufficiently large. For a heavy rope, i.e. $\gamma = 10^4$, the radius of the coil decreases monotonically as F is increased for the range of values tabulated. This may be explained by the fact that inertial effects, which cause the rope to balloon, become important only when $F = O(1)$. This effect is delayed further and further for heavier ropes. Reading table 2 vertically, we observe that as F is increased, l increases monotonically. This is consistent with the fact that for higher and higher feeding velocities, the rope starts to whirl with an increasing radius so that the rope length l increases. Reading tables 1 and 2 horizontally, we see that for fixed $F\gamma$, as γ is increased, R and l decrease monotonically. As γ becomes larger gravity dominates inertial and elastic effects, and the rope remains nearly vertical for most of its length.

In figure 2*a* we plot $\log R$ versus $\log F$ for $\gamma = 10$, 10^2, 10^3 and 10^4, and observe for large F, that $R \sim hF^{1/3}$. In figure 2*b* we plot $\log l$ versus $\log F$ for the same values of γ, and see that for large F, $l \sim hF^{1/2}$.

In figure 3*a* we plot $\log R$ versus $\log F$ for $F\gamma = 1$, 10, 10^2 and 10^3. For $F \ll 1$, we see that $R \sim hF^{1/3}$. Since $F\gamma$ is constant on each curve, then $R \sim h\gamma^{-1/3}$, in agreement with (2.4). In figure 3*b* we plot $\log l$ versus $\log F$ for the same values of $F\gamma$. For $F \ll 1$, we note that $l \sim h$.

The scaling regimes shown in figures 2 and 3 suggest that an asymptotic description of the coiling rope is valid for extreme values of the parameters F and γ. When $F\gamma \ll 1$ and $\gamma \ll 1$, the shape of the coiling rope is close to that shown in figure 1. In this case the stiffness is important along the entire length of the rope. When $F \gg 1$ or $F \ll 1$, corresponding to the cases of either inertia- or gravity-dominated coiling, the stiffness of the rope is relatively unimportant except in the regions near the feeding point and near the horizontal plane. In figures 4*a* and *b* we show the steady

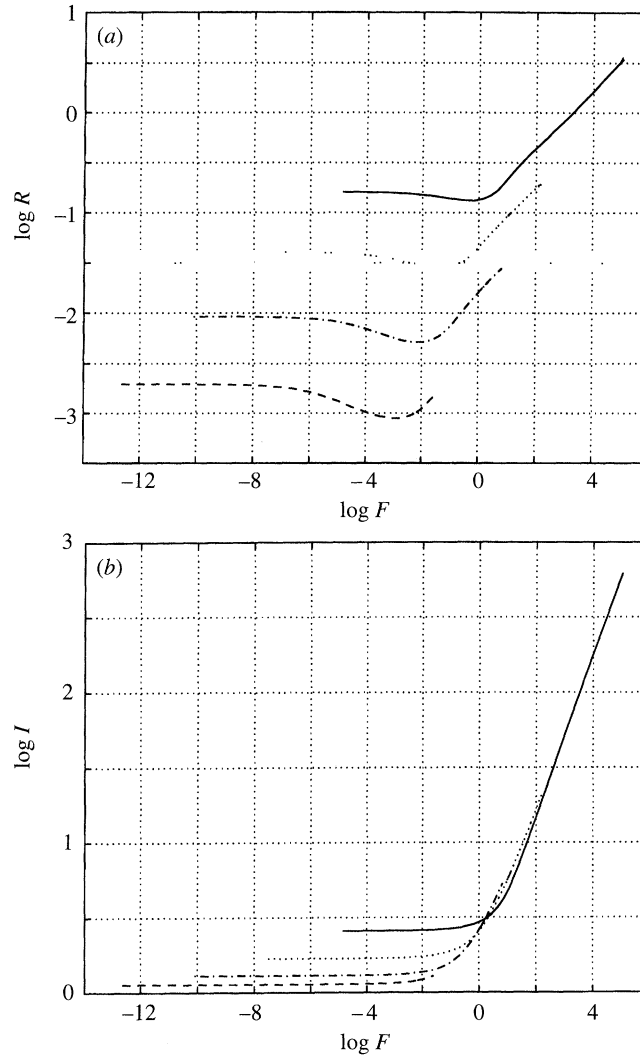

Figure 2. Dependence of (*a*) the dimensionless coil radius R and (*b*) the dimensionless rope length l on F, for: ——, $\gamma = 10$; · · · ·, $\gamma = 10^2$; – · –, $\gamma = 10^3$; – – –, $\gamma = 10^4$. Note the scaling regime for large values of F, i.e. inertia dominated coiling.

shape of a representative case from each regime corresponding to (*a*) a rapidly fed light coiling rope ($\gamma = 10$, $F = 1.5 \times 10^3$) and (*b*) a slowly fed heavy coiling rope ($\gamma = 10^4$, $F = 10^{-3}$) which is nearly vertical along most of its length.

In figure 4*c* we show the shape of a rapidly fed heavy coiling rope ($\gamma = 10^4$, $F = 10^{-1}$). Here the rope is nearly vertical in the region close to the feeding point, but balloons outwards close to the horizontal plane. This corresponds to the case when the bending stiffness is dominated by both inertia and gravity, with $F = O(1)$.

6. Asymptotic solution

A finite bending stiffness in the rope is necessary for the onset of coiling. However, its importance decreases when elasticity is dominated by gravity and inertia, and

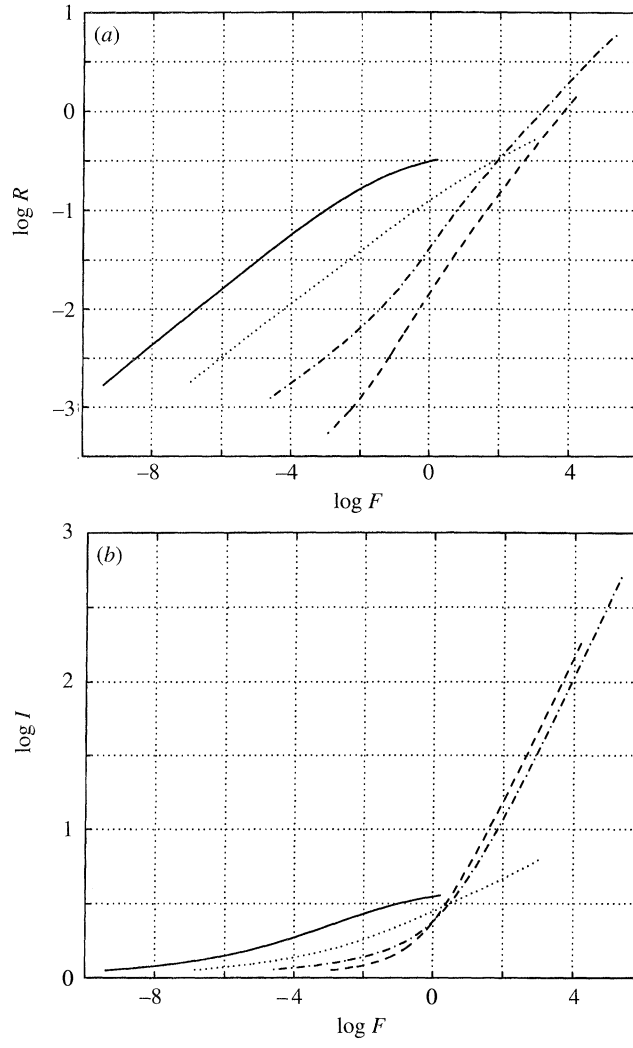

Figure 3. Dependence of (*a*) the dimensionless coil radius R and (*b*) the dimensionless rope length l on F, for: ——, $F\gamma = 1$; · · · ·, $F\gamma = 10$; – · –, $F\gamma = 10^2$; – – –, $F\gamma = 10^3$. Note the scaling regime for small values of F, i.e. gravity dominated coiling.

its effect is restricted to the boundary layers near the feeding point and near the horizontal plane. In the outer region away from the boundary layers, we can model the rope as a perfectly flexible string. However, since the coil radius R and the rope length l are determined by the competition between elastic and gravitational or inertial effects, we cannot predict these quantities without solving the exact equations.

For a perfectly flexible string, the bending or twisting stiffnesses are $EI \sim GJ \sim 0$. From (3.7) and the second equation in (3.6), it follows that $\boldsymbol{r}_s \times \boldsymbol{n} = 0$. Then the axial tension $\boldsymbol{n} = n\boldsymbol{r}_s$ is the only force that can be sustained by the string. Substituting the first equation in (4.1) into the first equation in (3.6), we get

$$\boldsymbol{n}_s + \rho A\boldsymbol{g} = -\rho A[v^2\boldsymbol{r}_{ss} - 2v\boldsymbol{\Omega} \times \boldsymbol{r}_s + \boldsymbol{\Omega} \times (\boldsymbol{\Omega} \times \boldsymbol{r})]. \tag{6.1}$$

This is the equation of motion for a perfectly flexible string moving at a constant speed v along its tangent and rotating about a fixed axis with angular velocity $\boldsymbol{\Omega}$.

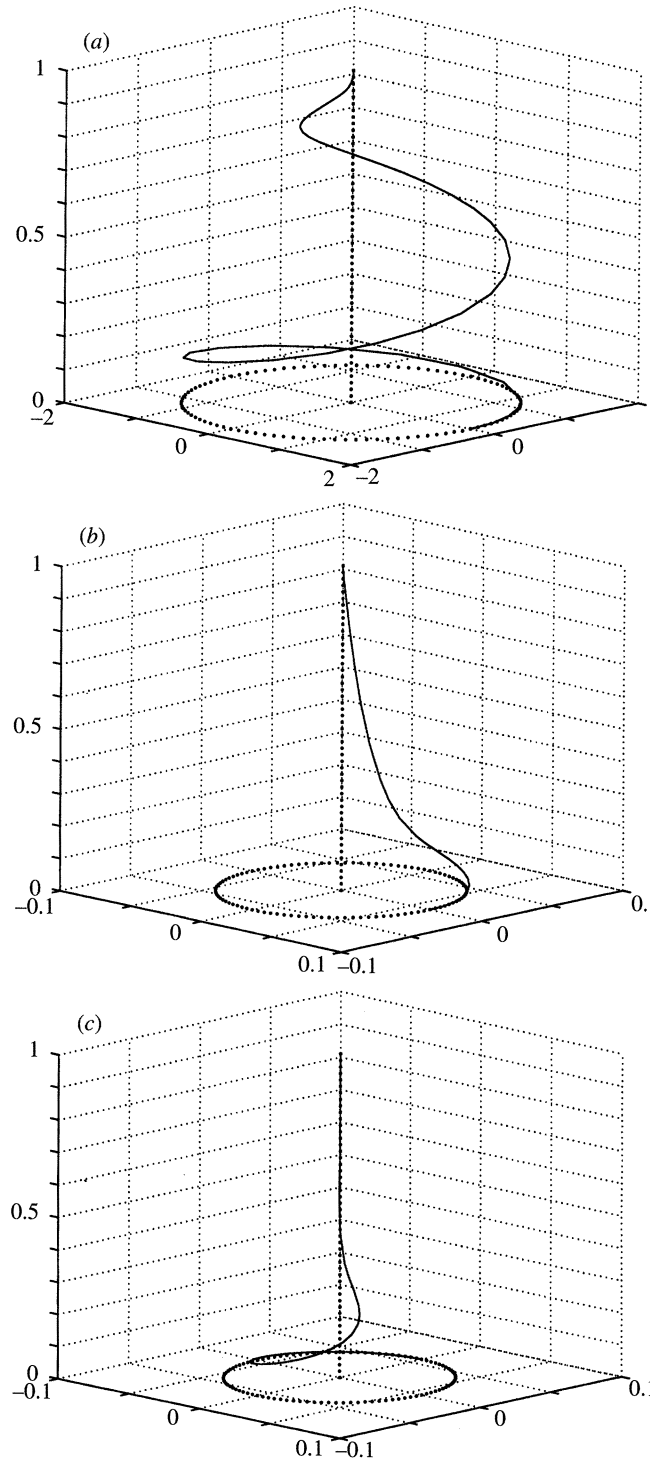

Figure 4. The instantaneous shape of a steadily coiling rope for (*a*) inertia-dominated coiling, $F = 1.5 \times 10^3$, $\gamma = 10$ (*b*) gravity-dominated coiling, $F = 10^{-3}$, $\gamma = 10^4$ and (*c*) inertia- and gravity-dominated coiling, $F = 10^{-1}$, $\gamma = 10^4$.

Here $\boldsymbol{r}(s)$ characterizes the centre line of the string, $\boldsymbol{\Omega} = \Omega \boldsymbol{e}_3$, $\boldsymbol{g} = -g\boldsymbol{e}_3$ and ρA is the mass per unit length of the string. In order to close the system (6.1) we need an additional equation for $n(s)$. Assuming that the string, like the rope considered previously, is inextensible gives

$$\boldsymbol{r}_s \cdot \boldsymbol{r}_s = 1. \tag{6.2}$$

Using the dimensionless variables $\bar{s} = s/l$, $\bar{x} = x/h$, $\bar{y} = y/h$, $\bar{z} = z/h$, $\bar{\Omega} = \Omega h/v$, $\bar{l} = l/h$, $F = v^2/gh$ and $\bar{n} = n/\rho A g h$, we can rewrite (6.1), (6.2), on dropping the bars, as

$$\left.\begin{aligned} (nx_s)_s = -F(x_{ss} + 2l\Omega y_s - l^2\Omega^2 x), \quad (ny_s)_s = -F(y_{ss} - 2l\Omega x_s - l^2\Omega^2 y), \\ (nz_s)_s = -Fz_{ss} + l^2, \quad x_s^2 + y_s^2 + z_s^2 = l^2. \end{aligned}\right\} \tag{6.3}$$

Here l is the length of the string, h is the height of the feeding point above the horizontal plane and F is the Froude number defined by the ratio of the kinetic energy to the gravitational potential energy. To derive an equation for the tension $n(s)$, we multiply the first three equations of (6.3) by x_s, y_s and z_s, respectively, and add them together. Using the inextensibility condition to simplify the resulting expression yields

$$n_s = F\Omega^2(xx_s + yy_s) + z_s. \tag{6.4}$$

This equation can be integrated immediately to yield

$$n(s) = F\Omega^2(x^2 + y^2) + z + n_0, \tag{6.5}$$

where n_0 is the constant of integration. The solutions of these equations for the drawing and whirling of a string have been investigated in Antman (1995) and Antman & Reeken (1987).

To complete the formulation of the outer problem we need some matching conditions that relate this solution to the inner solutions in the boundary layers. In the regions near the feeding point and near the horizontal plane, the bending stiffness cannot be neglected, and the boundary-layer equations of motion are obtained by rescaling the exact equations (4.6). These have to be solved numerically to derive matching conditions for the inner problem.

If the size of the boundary layers is very small, the outer solution should go from the feeding point to a point on the circle of radius R at $z = 0$. The corresponding boundary conditions at the feeding point $s = 0$ and the point of contact with the horizontal plane $s = 1$ are

$$x(1) = 0, \quad y(1) = 0, \quad z(1) = 1, \quad x(0) = R, \quad y(0) = 0, \quad z(0) = 0. \tag{6.6}$$

To solve the two-point boundary value problem given by (6.3) and (6.6), we have to specify the dimensionless coil radius $R \equiv x(0)$ and the dimensionless rope length l. Here, we will restrict our analysis to deriving the general form of the asymptotic solution.

When $\gamma \gg 1$ and $F = O(1)$, both inertia and gravity are important in determining the configuration of the rope in the region between the boundary layers. Figure 5 suggests that the form of the rope is similar to a catenary near the feeding point but changes to that of a helix near the horizontal plane. Therefore, we consider the following solution to (6.3):

$$x(s) = a \operatorname{sech} bs \cos \omega s, \quad y(s) = a \operatorname{sech} bs \sin \omega s, \quad z(s) = cs - d \tanh bs. \tag{6.7}$$

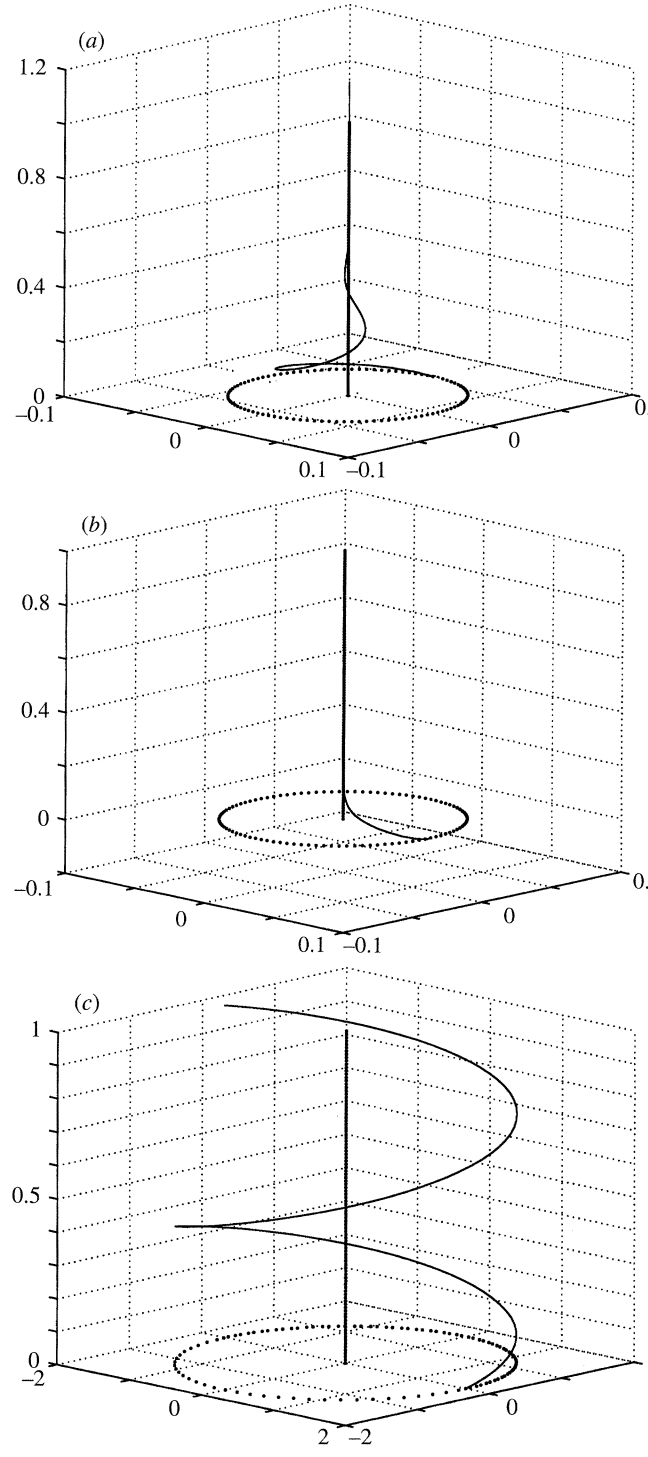

Figure 5. The asymptotic shape of a steadily coiling string for (*a*) $F = O(1)$, (*b*) $F \gg 1$, and (*c*) $F \ll 1$. These shapes are similar to those shown in figures 4*a*–*c*, respectively, except in the boundary layers near the feeding point and the horizontal plane.

Substituting (6.7) into the last equation in (6.3) gives the conditions $c = l$ and $a = d = 2bc/(b^2 + \omega^2)$ for the inextensibility constraint to be satisfied. The tension in the string is determined by substituting (6.7) into (6.5) and gives

$$n(s) = F\Omega^2 a^2 \operatorname{sech}^2 bs + (s - a \tanh bs) + n_0. \tag{6.8}$$

Figure 4*a* suggests that the form of the rope in inertia dominated motion, $F \gg 1$, is that of a whirling helix. Putting $b = 0$ in (6.7) gives

$$x(s) = a \cos \omega s, \quad y(s) = a \sin \omega s, \quad z(s) = cs. \tag{6.9}$$

Here a is the radius and c is the pitch of the helix. Substituting (6.9) into the last equation in (6.3) gives the condition $c = (l^2 - a^2\omega^2)^{1/2}$ for the inextensibility condition to be satisfied. Rescaling the tension $n(s)$ in (6.8) to absorb F, and letting $F \to \infty$ gives $n(s) = F\Omega^2 a^2 + n_0$.

Figure 4*b* suggests that the form of the rope in gravity dominated motion, $F \ll 1$, is that of a catenary. Putting $\omega = 0$ in (6.7) gives

$$x(s) = a \operatorname{sech} bs, \quad y(s) = 0, \quad z(s) = cs - d \tanh bs. \tag{6.10}$$

Substituting (6.10) into the last equation in (6.3) gives the conditions $c = l$ and $a = d = 2c/b$ for the inextensibility constraint to be satisfied. Letting $F \to 0$ in (6.8) gives the tension in the string: $n(s) = (s - a \tanh(2s/a)) + n_0$.

In figures 5*a*–*c* we show the asymptotic shape of the coiling rope in the outer region, corresponding to the string solution, given by (6.9), (6.10) and (6.7) for $F \gg 1$, $F \ll 1$ and $F = O(1)$, respectively. The values of l and $R = 1/\Omega$ in each case are chosen to be exactly the same as for the solutions shown in figures 4*a*–*c*. The parameters b and ω are chosen so that the boundary conditions at $s = 1$ are satisfied in each case. Of course this is not possible for the 'whirling helix' solution. We observe that the asymptotic shapes agree well with the shapes determined by solving the exact equations in the regions away from the boundary layers, i.e. away from the feeding point and the horizontal plane.

Appendix A. Euler angles and Euler parameters

In Kirchhoff–Love rod theory, the cross-section is characterized by specifying the orientation of an orthogonal triad fixed in the frame relative to another orthogonal triad fixed in space, as shown in figure 6. This requires a choice of some convenient parametrization of the group of rotations $SO(3)$.

Rotations are usually given in terms of the classical Euler angles denoted by ψ, θ and ϕ. However, this representation of the Euler angles breaks down at the polar singularities $\theta = 0, \pi$. To describe arbitrary rotations, we use a singularity-free parametrization in terms of the Euler parameters q_1, q_2, q_3, q_0 (Whittaker 1937, p. 9), which are just the components of the quaternions of Hamilton.

Here, we collect various expressions for the rotation matrices and the components of curvature and twist in terms of the Euler angles and Euler parameters for use in our analyses. The Euler angles are related to the Euler parameters by (Whittaker 1937, p. 11)

$$\left.\begin{aligned} q_1 &= \sin(\theta/2)\sin((\phi - \psi)/2), \quad & q_2 &= \sin(\theta/2)\cos((\phi - \psi)/2), \\ q_3 &= \cos(\theta/2)\sin((\phi + \psi)/2), \quad & q_0 &= \cos(\theta/2)\cos((\phi + \psi)/2), \end{aligned}\right\} \tag{A 1}$$

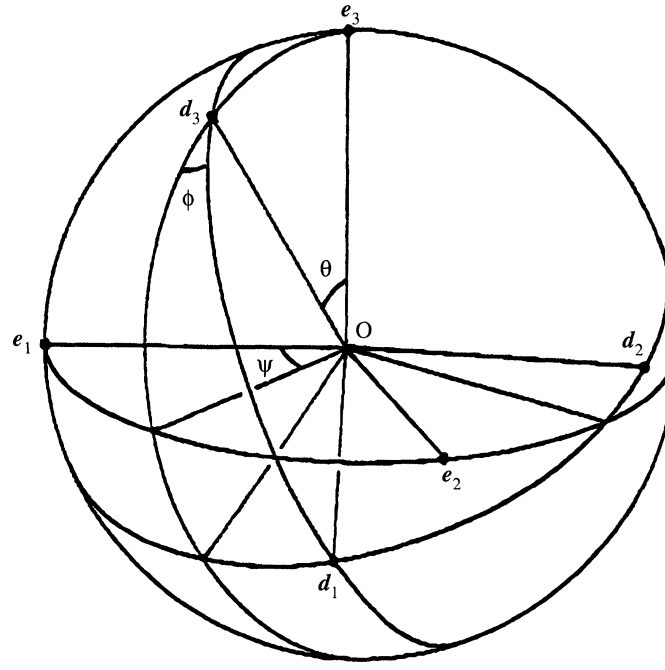

Figure 6. The Euler angles ψ, θ and ϕ determine the orientation of the moving coordinate axes $\boldsymbol{d}_1$, $\boldsymbol{d}_2$, $\boldsymbol{d}_3$ relative to the fixed coordinate axes $\boldsymbol{e}_1$, $\boldsymbol{e}_2$, $\boldsymbol{e}_3$. The tangent to the centre line of the rod is along $\boldsymbol{d}_3$, and the principal axes of the cross section are along $\boldsymbol{d}_1$ and $\boldsymbol{d}_2$.

where

$$q_1^2 + q_2^2 + q_3^2 + q_0^2 = 1. \tag{A 2}$$

In fact this relation between the Euler angles and the Euler parameters is a consequence of the isomorphism between the rotation group $SO(3)$ and the unitary group $SU(2)$.

In terms of the Euler parameters, the transformation matrix defined in (3.1) is given by (Whittaker 1937, p. 8)

$$\boldsymbol{L} = \begin{bmatrix} q_1^2 - q_2^2 - q_3^2 + q_0^2 & 2(q_1q_2 + q_0q_3) & 2(q_1q_3 - q_0q_2) \\ 2(q_1q_2 - q_0q_3) & -q_1^2 + q_2^2 - q_3^2 + q_0^2 & 2(q_2q_3 + q_0q_1) \\ 2(q_1q_3 + q_0q_2) & 2(q_2q_3 - q_0q_1) & -q_1^2 - q_2^2 + q_3^2 + q_0^2 \end{bmatrix}. \tag{A 3}$$

The components of the strain vector κ defined in (3.4) are (Whittaker 1937, p. 16)

$$\left.\begin{aligned} \kappa^{(1)} &= 2(q_0q_{1s} + q_3q_{2s} - q_2q_{3s} - q_1q_{0s}) \\ \kappa^{(2)} &= 2(-q_3q_{1s} + q_0q_{2s} + q_1q_{3s} - q_2q_{0s}) \\ \tau &= 2(q_2q_{1s} - q_1q_{2s} + q_0q_{3s} - q_3q_{0s}) \end{aligned}\right\} \tag{A 4}$$

To derive a system of first-order ordinary differential equations for the Euler parameters, we first differentiate (A 2) and get

$$0 = 2(q_1q_{1s} + q_2q_{2s} + q_3q_{3s} + q_0q_{0s}). \tag{A 5}$$

Inverting (A 4)–(A 5) yields the following first-order system of ordinary differential

equations for the Euler parameters

$$\left.\begin{aligned} q_{1s} &= \tfrac{1}{2}(q_0\kappa^{(1)} - q_3\kappa^{(2)} + q_2\tau), \quad & q_{2s} &= \tfrac{1}{2}(q_3\kappa^{(1)} + q_0\kappa^{(2)} - q_1\tau), \\ q_{3s} &= \tfrac{1}{2}(-q_2\kappa^{(1)} + q_1\kappa^{(2)} + q_0\tau), \quad & q_{0s} &= \tfrac{1}{2}(-q_1\kappa^{(1)} - q_2\kappa^{(2)} - q_3\tau). \end{aligned}\right\} \tag{A 6}$$

Finally, we write the first-order ordinary differential equations for the coordinates of the centre line of the rod $x(s)$, $y(s)$ and $z(s)$. In terms of the Euler parameters they are

$$x_s = 2(q_1q_3 - q_0q_2), \quad y_s = 2(q_2q_3 + q_0q_1), \quad z_s = -q_1^2 - q_2^2 + q_3^2 + q_0^2. \tag{A 7}$$

We thank Professor E. J. Doedel for providing us with a copy of the numerical bifurcation analysis package AUTO (Doedel 1986).

References

Antman, S. S. 1995 *Problems of nonlinear elasticity.* Berlin: Springer.

Antman, S. S. & Reeken, M. 1987 Whirling and drawing of strings. *SIAM Jl Math. Analysis*, **18**, 337–365.

Doedel, E. J. 1986 AUTO, software for continuation and bifurcation analysis of BVPs. Department of Computer Science, Concordia University.

Griffiths R. W. & Turner, J. S. 1988 Folding of viscous plumes impinging on a density or viscosity interface. *Geophys. Jl* **95**, 397–419.

Struik, D. J. 1988 *Lectures on classical differential geometry.* New York: Dover.

Taylor, G. I. 1969 Instability of jets, threads and sheets of viscous fluid. *Proc. 12th Int. Cong. on Applied Mechanics*, pp. 382–395.

Tchavdarov, B., Yarin, A. L. & Radev, S. 1993 Buckling of thin liquid jets. *J. Fluid Mech.*, **253**, 593–615.

Whittaker, E. T. 1937 *A treatise on the analytical dynamics of particles and rigid bodies.* Cambridge University Press.

Received 20 March 1995; revised 19 June 1995; accepted 27 June 1995